

On the Behavior of Water at Subfreezing Temperatures in a Protein Crystal: Evidence of Higher Mobility Than in Bulk Water

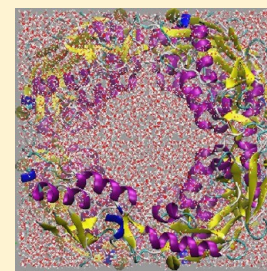
Dongqi Wang*,†,⊥ Anja Böckmann,‡ Jožica Dolenc,† Beat H. Meier,† and Wilfred F. van Gunsteren*,†

†Laboratory of Physical Chemistry, ETH Zürich, CH-8093 Zürich, Switzerland

‡Institut de Biologie et Chimie des Protéines, Université de Lyon, 69367 Lyon, France

S Supporting Information

ABSTRACT: NMR experiments have shown that water molecules in the crystal of the protein Crh are still mobile at temperatures well below 273 K. In order to investigate this water anomaly, a molecular dynamics (MD) simulation study of crystalline Crh was carried out to determine the mobility of water in this crystal. The simulations were carried out at three temperatures, 150, 200, and 291 K. Simulations of bulk water at these temperatures were also done to obtain the properties of the simple point charge (SPC) water model used at these temperatures and to allow a comparison of the properties of water in the Crh crystal with those of bulk water at the same temperatures. According to the simulations, water is immobilized at 150 K both in crystal and in bulk water. As expected, at 291 K it diffuses and rotates more slowly in the protein crystal than in bulk water. However, at 200 K, the translational and rotational mobility of the water molecules is larger in the crystal than in bulk water. The enhancement of water mobility in the crystal at 200 K was further investigated by MD simulations in which the backbone or all protein atoms were positionally restrained, and in which additionally the electrostatic protein–water interactions were removed. Of these changes in the environment of the water molecules, rigidifying the protein backbones slightly enhanced water diffusion, while it slowed down rotation. In contrast, removal of electrostatic protein–water interactions did not change water diffusion but enhanced rotational motion significantly. Further investigations are required to delineate particular features of the protein crystal that induce the anomalous behavior of water at 200 K.



INTRODUCTION

Water is ubiquitous in biomolecular systems. This is likely to be due to its particular physical–chemical properties at a physiological range of temperatures and pressures, such as a high entropy of about half as much as its energy when divided by the temperature, its density maximum at 4 °C, its strong capacity to solvate ions, and its capability to make up to four hydrogen bonds. For a long time, the structural basis of these particular properties was not well understood at the molecular level because only averages over many molecules in the bulk could be measured, which for the liquid phase do not uniquely determine the structural or configurational statistical–mechanical ensemble of water. This allowed the proposition of a great variety of molecular models for liquid water,¹ of which the most extravagant was that of so-called poly water, i.e., water as a polymer.²

The advent of molecular dynamics (MD) computer simulation,^{3,4} which allowed the generation of statistical–mechanical ensembles and the proper calculation of ensemble averages, offered some 40 years ago the opportunity to test simple molecular models for water that could reproduce many of its properties.⁵ Since then our understanding of the peculiar properties of water has been enhanced due to the development of a great many molecular models for water,⁶ from simple ones such as simple point charge (SPC)⁷ that grasp the most important thermodynamic, dielectric, and hydrogen bonding properties of water in the liquid phase at physiological temperatures and pressures to complex models^{8–11} that aim

at a reproduction of as many as possible properties of water in the gas, liquid, and solid phases.

Water plays an essential role in molecular biology because it allows biomolecules such as proteins and RNA to adopt a particular three-dimensional structure in which they can exert their function and appears as well as an integral part of protein–protein,^{12,13} protein–DNA,^{14,15} and protein–ligand^{16,17} interactions. The interaction of water with its cosolvents such as ions or organic molecules allows it on the other hand to induce unfolding or denaturation of the protein or RNA molecules. In contrast to crystals of small biomolecules, a crystal of a protein can contain considerable amounts of water, e.g., 67% for the crystals investigated in this paper, Crh (protein catabolite repression Hpr;^{18,19} see Figure 1). This has raised the question whether this water behaves as bulk (or neat) water or whether its behavior is modified by the presence of the protein molecules.

Experimentally, NMR measurements have produced evidence that water that remains with the crystals of Crh upon ultracentrifugation does not freeze at 0 °C but remains mobile down to at least –30 °C.²⁰ An experimental ²H NMR relaxation study of the rotational dynamics of water molecules in hydrophobic hydration shells of four partially hydrophobic solutes at temperatures between 243 and 308 K found that

Received: January 20, 2013

Revised: August 31, 2013

Published: September 2, 2013

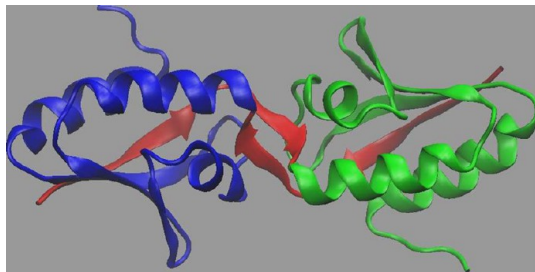


Figure 1. Crystal structure of a Crh dimer with the monomers shown in blue and green. The residues at the N-terminal parts of the protein connecting the monomers are shown in red. The residues 12–14 in the center of the dimer have a β_{1a} secondary structure.

below 255 K hydrophobic hydration water rotates faster than bulk water.²¹ Computationally, the properties of water in a nanoconfinement, e.g., between two hydrophobic walls, has been studied by different groups,^{22–24} and changed behavior was found for small confinements with respect to phase transitions,²⁴ the dipole moment,^{25,26} the dielectric constant,²⁷ orientational dynamics in the core and at the interface of a nanodroplet,²⁸ its impact on protein kinetics and thermodynamics (folding),²⁹ the density maximum and minimum,³⁰ thermal expansion,³¹ connectivity pattern,³² librational motions,³³ structure,³⁴ and the viscosity.^{35,36} Simulations of water with solutes in different concentrations show the translational and rotational dynamics to be dependent on solute concentration.^{37,38}

The mutual influence of water and a protein with respect to their atomic mobilities was investigated using MD simulations in which the protein and the water were kept alchemically at different temperatures.^{39–41} It appeared that the temperature of the water has a strong influence on the positional fluctuations of the protein atoms. The influence of protein mobility and electrostatic protein–water interactions upon water mobility in the protein hydration shell has been analyzed for the protein hen egg white lysozyme in aqueous solution at 300 K.⁴² Rigidifying the protein appears to slow down water diffusion, while without electrostatic interactions with the protein, water reorientation is faster than in bulk water.

Crystals formed by Crh contain about 780 H₂O molecules and ions per protein monomer consisting of 87 amino acid

residues. The P₄₃₂₂ crystal unit cell contains large water-filled channels between the different protein molecules (Figure 2) in which H₂O molecules are able to diffuse more or less freely. In order to investigate the properties of water in this crystal, we have simulated a full unit cell of Crh containing 8 dimers of the protein, i.e., sixteen 87-residue proteins, 96 Na⁺ ions, 24 SO₄²⁻ ions, and 12 203 H₂O molecules, at different temperatures of 150, 200, and 291 K, and analyzed the translational and rotational mobility of the water molecules in this crystal. Since the water model used in the simulation is expected to determine the behavior of water in the crystal simulation, we have carried out simulations of bulk water at the same temperatures and using the same water model. The properties of water as obtained from these simulations of bulk water are used as reference to which the properties of water in the Crh crystal are compared.

The simulations show an enhanced mobility of water in the Crh crystal at temperatures below the freezing temperature of bulk water. This phenomenon is further analyzed by repeating the crystal simulations under different conditions: with the protein backbones kept fixed, or in addition the side chains kept fixed, or in addition with the electrostatic interactions between water and protein switched off.

■ COMPUTATIONAL DETAILS

Construction of the Unit Cell. The X-ray crystal structure of Crh (PDB code: 1MU4,¹⁹ resolution: 1.80 Å) was used to construct a unit cell of the protein. In the crystal structure, the proteins appear as a dimer with the N-termini of the two monomers forming an antiparallel β -sheet with each other, in the presence of 3 SO₄²⁻ ions and 122 H₂O molecules. Eight replicas were generated by means of symmetry transformations of the dimer, together with the crystallographic ions and water molecules, to obtain the unit cell with a symmetry of P₄₃₂₂ to be used in the simulations.

The residues were protonated according to a pH of 7. The histidine residues were protonated at N_δ or at N_η according to their hydrogen-bonding environment. This led to a total charge of $-6e$ per protein dimer. After the protonation of the residues, the unit cell was solvated in a SPC⁷ water box. In the crystal, the solvent content (V_s) was measured as 66.82%, with a Matthews coefficient (V_M) of 3.71 Å³·Da⁻¹. In order to solvate

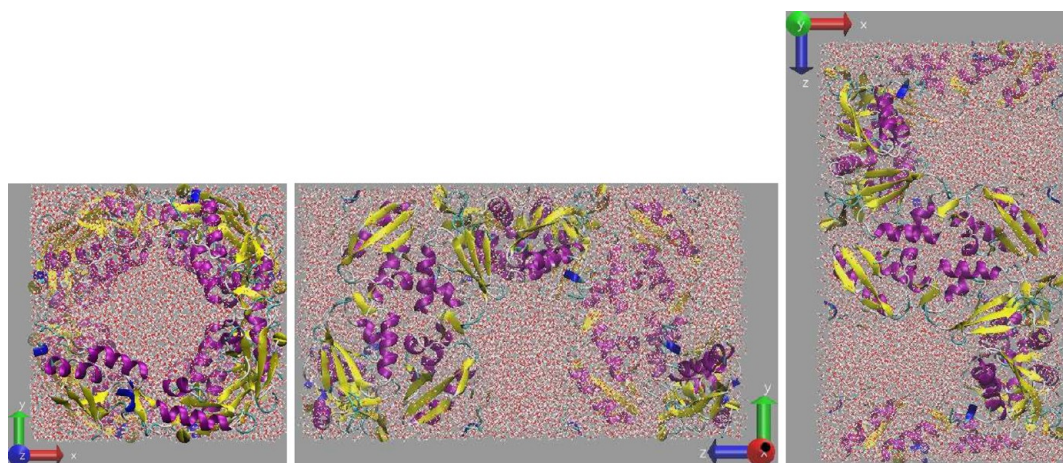


Figure 2. Rectangular unit cell containing 16 Crh proteins, 12 203 water molecules, and 120 ions, seen along the z-axis (left panel), along the x-axis (middle panel), and the y-axis (right panel). The edge lengths are 6.885 nm (red and green arrows) and 11.986 nm (blue arrow).

Table 1. Simulations

simulation name	system ^a	ensemble ^b	T [K]	length [ns]	position restraints ^c	protein partial charges ^d
neat_V_100	bulk water	V	100	3		
neat_V_150	bulk water	V	150	3		
neat_V_200	bulk water	V	200	3		
neat_V_250	bulk water	V	250	3		
neat_V_291	bulk water	V	291	3		
neat_V_300	bulk water	V	300	3		
neat_P_100	bulk water	P	100	3		
neat_P_150	bulk water	P	150	3		
neat_P_200	bulk water	P	200	3		
neat_P_250	bulk water	P	250	3		
neat_P_291	bulk water	P	291	3		
neat_P_300	bulk water	P	300	3		
cry_V_150	Crh crystal	V	150	19		ff
cry_V_200	Crh crystal	V	200	19		ff
cry_V_291	Crh crystal	V	291	19		ff
cry_V_200_br	Crh crystal	V	200	19	b	ff
cry_V_200_pr	Crh crystal	V	200	19	p	ff
cry_V_200_prp0	Crh crystal	V	200	19	p	0
cry_V_200_prp0i0	Crh crystal	V	200	19	p	0
cry_V_291_br	Crh crystal	V	291	19	b	ff
cry_V_291_pr	Crh crystal	V	291	19	p	ff
cry_V_291_prp0	Crh crystal	V	291	19	p	0
cry_V_291_prp0i0	Crh crystal	V	291	19	p	0

^aThe composition of the simulated system: Crh crystal or bulk water. ^bThe ensemble employed, where P represents isobaric, and V constant volume.^cPositional restraints used in the simulations. ^dThe partial charge on protein atoms, where 0 represent zero charge, and ff the partial charges from the force field.

the protein at a similar hydration level as in the crystalline Crh, an interatomic distance threshold between non-hydrogen protein and water atoms was chosen (0.22 nm) to control the number of solvent molecules present in the unit cell as derived from the Matthew relation.⁴³

After the relaxation of the solvent positions during which the protein was kept fixed, 96 H₂O molecules at positions with the largest negative potential values were replaced by Na⁺ ions to neutralize the negative charge of 8 × 6e of the system due to the deprotonated titratable residues and the 24 crystallographic SO₄²⁻ ions. This unit cell was then subjected to the thermalization (1 ns) and sampling (19 ns) at the temperatures 150, 200, and 291 K.

Simulations. All MD simulations of the crystalline Crh were carried out using the GROMOS 45A3 force field,⁴⁴ involving a united-atom description of aliphatic groups, and the SPC water model.⁷ The simulations were performed using the GROMOS software^{45–48} under minimum image periodic boundary conditions based on rectangular computational boxes of edge lengths 6.885, 6.885, and 11.986 nm, containing eight dimers of Crh, 24 SO₄²⁻, 96 Na⁺, and 12 203 H₂O molecules at constant volume and at 150, 200, and 291 K. The choice to simulate the crystal at a constant volume measured at 291 K instead of at a constant pressure was based on the consideration to avoid a deformation of the crystal and the positions of the protein atoms due to force-field inaccuracies that would affect the protein–water interactions. Indeed, 1 ns MD simulations at 200 K and constant pressure showed a slight deformation of the crystal unit cell, with the cell lengths *a* and *b* increasing by about 0.4% and the cell length *c* decreasing by about 3.2% leading to a decrease in volume of 2.7%. This value is of the same order of magnitude as the deviation of the density of SPC water from the experimental value at ambient

temperature and pressure. In the constant volume simulations, the protein structure was thus preserved at the price of having a slightly too low pressure at the lower temperatures: −859 kJ mol^{−1} nm^{−3} at 150 K, −812 kJ mol^{−1} nm^{−3} at 200 K, and +114 kJ mol^{−1} nm^{−3} at 291 K. Because of the small size of the computational boxes used in MD simulations and the large incompressibility of water and proteins, the pressure fluctuations are larger, about 1000 kJ mol^{−1} nm^{−3}, than the average pressures. Finally, a comparison of the properties of bulk SPC water at constant volume and at constant pressure (see Figures 6, 16, and 17) show qualitatively the same behavior of bulk water under these different simulation conditions.

The leapfrog algorithm⁴⁹ was used to integrate Newton's equations of motion with a time step of 2 fs. Solute bond-length constraints as well as the rigidity of the water molecules were enforced by application of the SHAKE procedure⁵⁰ with a relative geometric tolerance of 10^{−4}. The nonbonded interactions were computed using a triple-range scheme,^{45,46} with short- and long-range cutoff distances set to 0.8 and 1.4 nm, respectively, and an update frequency of 5 time steps for the short-range pairlist and intermediate-range interactions. A reaction-field force^{51,52} was applied to account for the mean effect of electrostatic interactions beyond the long-range cutoff distance, using a relative dielectric permittivity of 61 as appropriate for the SPC water model.⁵³ The temperature was maintained close to its reference value by weakly coupling solute and solvent degrees of freedom separately to external baths⁵⁴ using a relaxation time of 0.1 ps. The translation of the box center of mass was removed every 1000 time steps. Simulations of bulk water at constant volume (NVT) and at constant pressure (NPT) were started from a cubic box of initial edge length 5.493 nm, containing 5384 SPC water molecules.

Table 2. Diffusion Coefficient D (in 10^{-5} nm 2 ps $^{-1}$), Rotational Relaxation Times τ_l , $l = 1, 2$ (in ps) $\tau_1(OH_1)$, $\tau_1(OH_2)$, $\tau_1(H_1H_2)$, and $\tau_1(\mu)$ for the Vectors O–H₁, O–H₂, H₁–H₂, and the Dipole Moment μ of Water Molecules in the Crh Crystal and in Bulk Water^a

simulation name	D	$\tau_1(OH_1)/\tau_2(OH_1)$	$\tau_1(OH_2)/\tau_2(OH_2)$	$\tau_1(H_1H_2)/\tau_2(H_1H_2)$	$\tau_1(\mu)/\tau_2(\mu)$
Crh crystal					
cry_V_150	0.2	inf/inf	inf/inf	inf/inf	inf/inf
cry_V_200	8.7	400/165	405/167	347/212	565/149
cry_V_291	114	4.0/1.4	4.0/1.4	3.8/1.5	4.5/1.1
bulk water					
neat_V_150	0.4	inf/inf	inf/inf	inf/inf	inf/inf
neat_V_200	2.4	857/424	867/425	796/526	1020/374
neat_V_291	379	3.0/1.0	3.0/1.0	3.0/1.1	3.0/0.8
neat_V_300	443	2.5/0.8	2.5/0.8	2.5/0.9	2.6/0.7
neat_P_150	0.4	inf/inf	inf/inf	inf/inf	inf/inf
neat_P_200	3.3	464/217	460/216	434/264	524/186
neat_P_291	377	3.0/1.0	3.0/1.0	2.9/1.1	3.0/0.8
neat_P_300	436	2.5/0.9	2.5/0.9	2.5/0.9	2.6/0.7

^aThe values were determined from 3 ns time periods and averaged over all 12 203 (Crh crystal) or 5384 (bulk water) molecules. Inf: the value could not be reliably determined from the finite simulation period.

Table 3. Diffusion Coefficient D (in 10^{-5} nm 2 ps $^{-1}$), Rotational Relaxation Times τ_l , $l = 1, 2$ (in ps) $\tau_1(OH_1)$, $\tau_1(OH_2)$, $\tau_1(H_1H_2)$, and $\tau_1(\mu)$ for the Vectors O–H₁, O–H₂, H₁–H₂, and the Dipole Moment μ of Water Molecules in the Crh Crystal and in Bulk Water as a Function of a Variation of the Environment^a

simulation name	D	$\tau_1(OH_1)/\tau_2(OH_1)$	$\tau_1(OH_2)/\tau_2(OH_2)$	$\tau_1(H_1H_2)/\tau_2(H_1H_2)$	$\tau_1(\mu)/\tau_2(\mu)$
neat_V_200	2.4	857/424	867/425	796/526	1020/374
neat_P_200	3.3	464/217	460/216	434/264	524/186
cry_V_200	8.7	400/165	405/167	347/212	565/149
cry_V_200_br	9.8	445/182	453/183	381/239	668/165
cry_V_200_pr	8.8	499/209	508/212	414/281	802/196
cry_V_200_prp0	9.4	177/74	178/75	152/93	257/72
cry_V_200_prp0i0	9.4	170/74	170/74	154/90	212/67
neat_V_291	379	3.0/1.0	3.0/1.0	3.0/1.1	3.0/0.8
neat_P_291	377	3.0/1.0	3.0/1.0	2.9/1.1	3.0/0.8
cry_V_291	114	4.0/1.4	4.0/1.4	3.8/1.5	4.5/1.1
cry_V_291_br	224	4.0/1.4	4.0/1.4	3.8/1.5	4.6/1.1
cry_V_291_pr	213	4.2/1.7	4.2/1.6	3.9/1.7	4.9/1.5
cry_V_291_prp0	213	3.3/1.3	3.3/1.3	3.1/1.2	3.8/1.0
cry_V_291_prp0i0	204	3.2/1.2	3.2/1.2	3.1/1.7	3.5/0.8

^aThe values were determined from 1 ns time periods and averaged over all 12 203 (Crh crystal) or 5384 (bulk water) molecules. *V*: constant volume; *P*: constant pressure; *br*: protein backbone atoms are positionally restrained; *pr*: all protein atoms are positionally restrained; *p0*: partial charges on protein atoms set to zero; *i0*: partial charges on atoms of ions set to zero.

The set of simulations in this work, 23 in total, differ from each other with respect to temperature, pressure and Hamiltonian. The crystal was simulated at 150, 200, and 291 K. To clarify the influence of the protein on the motion of water, additional simulations were performed while keeping the backbone atoms, or all protein atoms harmonically positionally restrained using a force constant of 1000 kJ mol $^{-1}$ nm $^{-2}$. To investigate the influence of the partial charges of the protein on the water mobility these partial charges were additionally set to zero in an additional simulation. In another simulation, the partial charges of the ions were additionally set to zero. These simulations are labeled as cry_V_X[_Y] in Table 1 where X represents the temperature, and Y the atoms that are restrained and the charge setting: *br*: backbone restrained, *pr*: protein restrained, *pp0*: protein restrained with all protein atoms having zero atomic charge, *pp0i0*: *pp0* plus zero atomic charge for ions; that is, SO₄²⁻ and Na⁺ appear as uncharged Lennard-Jones particles. For the simulation of bulk water, temperatures of 100, 150, 200, 250, 291, and 300 K were used. These

simulations are labeled as neat_X_Y in Table 1 where X represents V (constant volume) or P (constant pressure), and Y the temperature.

Analysis. The simulation trajectories were analyzed to characterize the motion of the protein atoms and water molecules. The properties that have been analyzed include the atom-positional root-mean-square deviation (RMSD) of the protein atoms from their initial positions (Figure 3), the atom-positional root-mean-square fluctuations (RMSF) of the protein atoms (Figure 5), the secondary structure of the proteins (Figure 4) according to the Dictionary of Secondary Structure of Protein (DSSP)⁵⁵ protocol for proteins, and for water the oxygen atom-positional RMSF (Figures 6 and 7), the oxygen–oxygen radial distribution function (RDF) (Figure 16), the density ρ (Figure 17), the heat capacity C_p (Figure 17), the thermal expansion coefficient α_p (Figure 17), the diffusion coefficient (D) (Tables 2 and 3), and the rotational relaxation times (τ_1 and τ_2) (Tables 2 and 3, Figures 14 and 15) of the water molecules. These properties have been calculated as in ref

56 except for the diffusion coefficient and the rotational relaxation time which were calculated as specified below.

Diffusion Coefficient. The diffusion coefficient, D_i , of the water molecules was calculated

$$D_i = \lim_{t \rightarrow \infty} \frac{\langle [\vec{r}_i(\tau + t) - \vec{r}_i(\tau)]^2 \rangle_\tau}{6 \cdot t} \quad (1)$$

where $\vec{r}_i(t)$ is the position of the oxygen of a water molecule i at time t , and the averaging indicated by $\langle \dots \rangle$ is over initial times τ .

Rotational Relaxation Time. The first- and second-order Legendre rotational relaxation times τ_1 and τ_2 are obtained from the autocorrelation function of the Legendre polynomials P_l of molecular vector \vec{e}_i^α of molecule i ,

$$C_{li}^\alpha(t) = \langle P_l(\vec{e}_i^\alpha(t') \cdot \vec{e}_i^\alpha(t' + t)) \rangle_t \quad (2)$$

The vectors \vec{e}_i^α considered include $\vec{r}_{H_1O} = \vec{r}_{H_1} - \vec{r}_O$, $\vec{r}_{H_2O} = \vec{r}_{H_2} - \vec{r}_O$, $\vec{r}_{H_1H_2} = \vec{r}_{H_1} - \vec{r}_{H_2}$, and $\vec{\mu}$, the dipole moment of water molecule i .

We analyze the fast relaxation of water rotational motion by assuming it to be exponential for times smaller than τ_{li}^α

$$C_{li}^\alpha(t) = \exp(-t/\tau_{li}^\alpha) \quad (3)$$

so τ_{li}^α was obtained from

$$\ln(C_{li}^\alpha(\tau_{li}^\alpha)) = -1 \quad (4)$$

Determination of the slow relaxation is hampered by low statistics for single molecules, for which reason it is not analyzed here.

RESULTS AND DISCUSSION

Structure and Mobility of the Proteins. Deviation from the X-ray Structure. The atom-positional RMSDs from the X-ray structure for the backbone atoms (C, C_α, N) of the nonterminal residues (4–84) of each monomer in the simulations at 150, 200, and 291 K are shown in Figure 3.

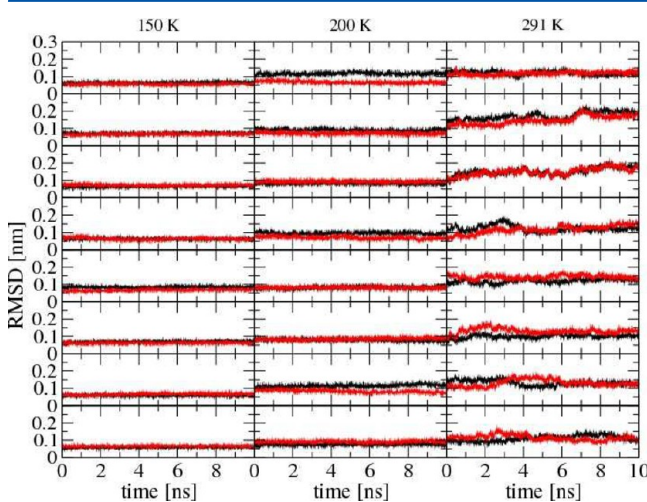


Figure 3. Positional root-mean-square deviation for the backbone atoms of nonterminal residues (4–84) with respect to the X-ray structure¹⁹ 1MU4 for the eight dimers (top to bottom panels) in the unit cell as a function of time for the final 10 ns of the simulations cry_V at 150, 200, and 291 K (from left to right). Red: first monomer, black: second monomer of a dimer.

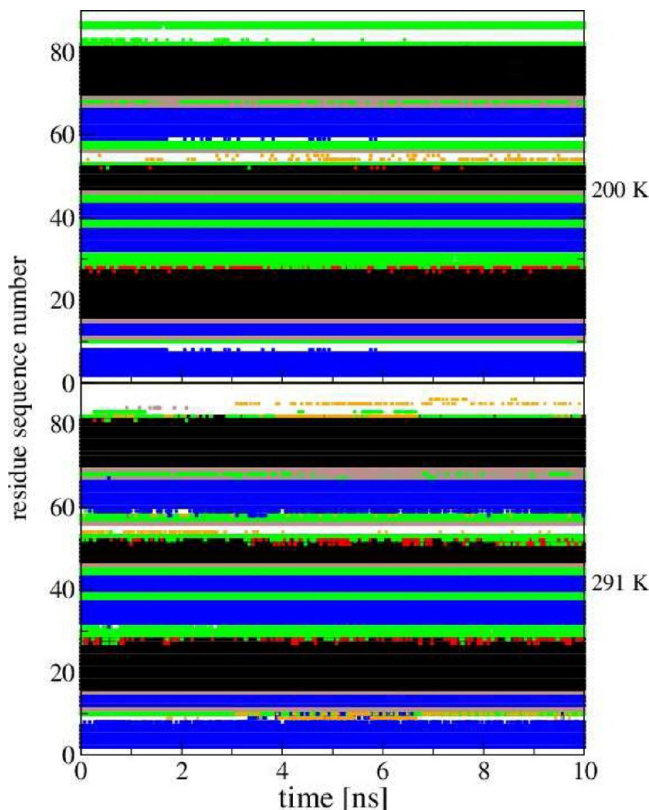


Figure 4. Secondary structure⁵⁵ of the protein Crh, monomer 1 in the crystal, as a function of time for the final 10 ns of the simulations cry_V_200 ($T = 200$ K, upper panel) and cry_V_291 ($T = 291$ K, lower panel). The simulation names are defined in Table 1. Black: α -helix; red: 3₁₀-helix; green: bend; gray: turn; blue: β -strand; yellow: bridge.

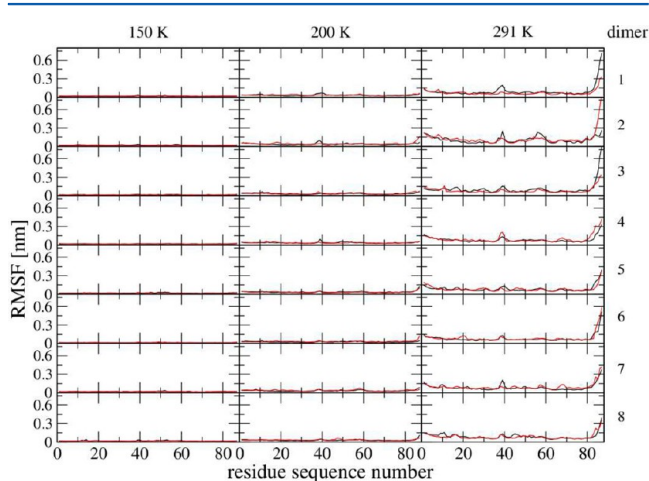


Figure 5. Backbone C_α positional root-mean-square fluctuation of the 16 monomers (from top to bottom) of Crh in the three simulations at 150, 200, and 291 K (from left to right). In each panel, the first monomer of each dimer is represented in black and the other one in red.

The crystal structure determined at 297 K was taken as the reference in the calculations of the RMSD.

The analysis shows that at low temperature (150 K) the proteins are immobilized with an RMSD of 0.05–0.07 nm. Raising the temperature enhances their mobility, and at 200 K they are observed to have an RMSD of around 0.1 nm. When

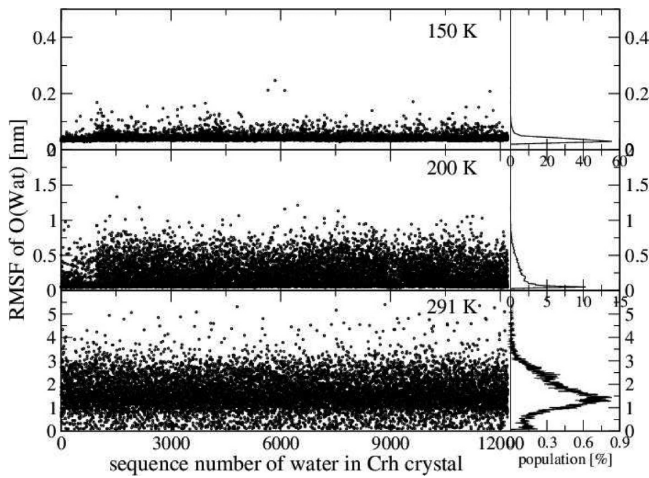


Figure 6. Atom-positional root-mean-square fluctuations over a 1 ns period of the oxygen atoms of the 12 203 water molecules in the crystal of Crh and their distribution for the three simulations at 150, 200, and 291 K (top to bottom).

the temperature goes up to 291 K, the simulation yields an RMSD of 0.1–0.2 nm for the backbone atoms of the nonterminal residues.

Secondary Structure of the Proteins. The analysis of secondary structure is based on the DSSP protocol.⁵⁵ Experimentally, a monomer is considered to have eight secondary structure units, including β_1 (residues 2–8), β_{1a} (residues 12–14), helix A (residues 16–27), β_2 (residues 32–37), β_3 (residues 40–43), helix B (residues 47–52), β_4 (residues 59–66), helix C (69–82), among which β_{1a} is a short β -strand forming a β -sheet with the β_{1a} -strand of the other monomer of a dimer.

The time series 9–19 ns of the secondary structure of one monomer in the simulations at 200 and 291 K is shown in Figure 4. The other 15 monomers show similar behavior. The secondary structure is stable during the simulations. The mobility of the proteins slightly increases with higher temperature, but at 291 K the secondary structure is only moderately perturbed. The result from the simulation at 150 K is not shown since the proteins are immobilized at such a low temperature.

Atom-Positional Fluctuations. The atom-positional root-mean-square fluctuation (RMSF) of the C_α atoms of the 87 residues of each monomer are shown in Figure 5. The protein is immobilized at 150 K. At 200 K, mobility is observed for residues 38 and 39 and the C-terminus, and at 291 K the fluctuations are 0.1–0.2 nm. Residues 38 and 39 connect a short secondary structure, the β_2 strand (residues 32–37) with

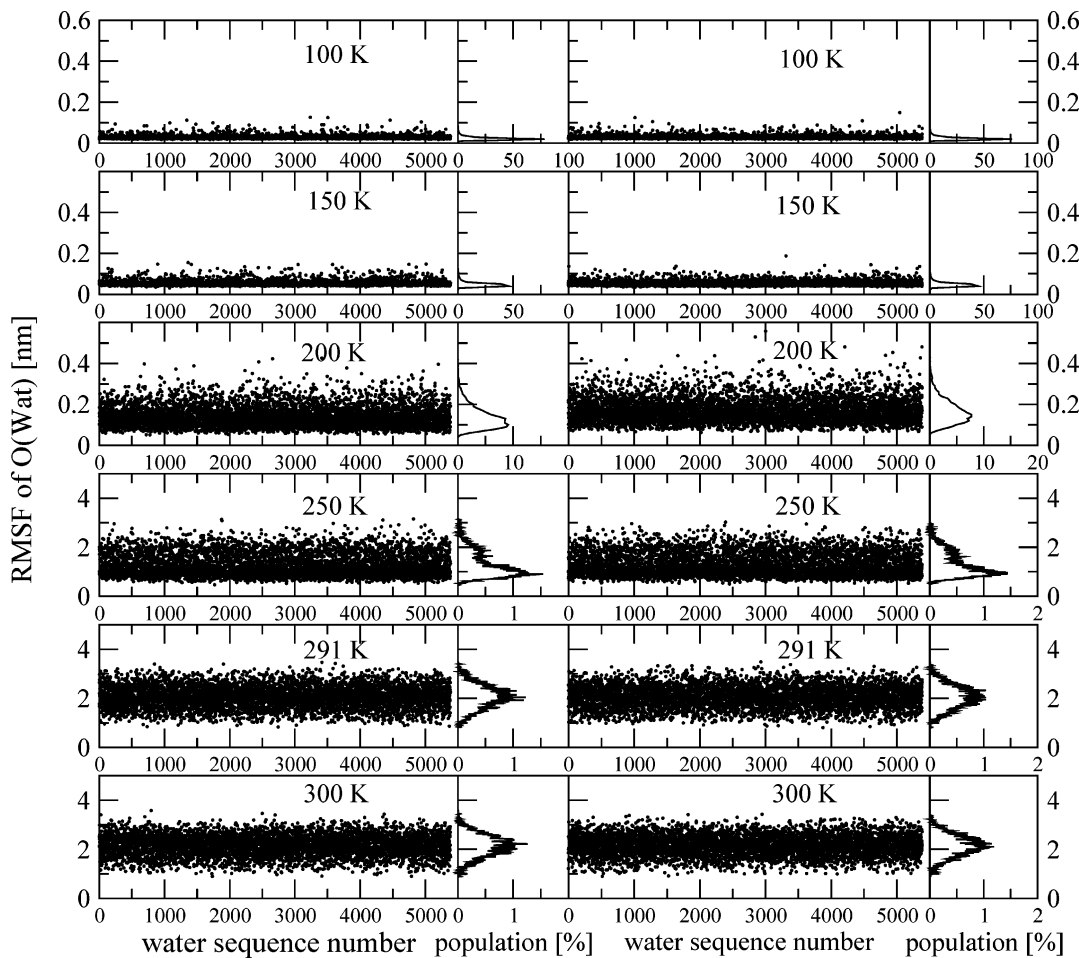


Figure 7. Atom-positional root-mean-square fluctuations over a 1 ns period of the oxygen atoms of 5384 water molecules in bulk water and their distribution in the simulations at constant volume (left panels) and constant pressure (right panels) at 100, 150, 200, 250, 291, and 300 K (top to bottom).

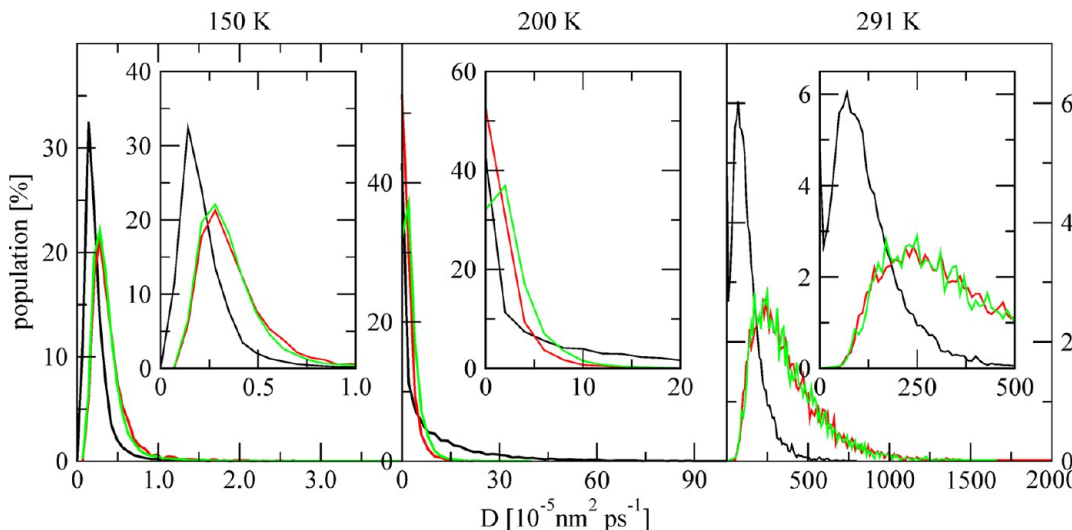


Figure 8. The distribution of the diffusion coefficients D of water molecules in the Crh crystal (in black) and in bulk water (in red for constant volume and in green for constant pressure). The inset of each panel enlarges the distribution for low values of D .

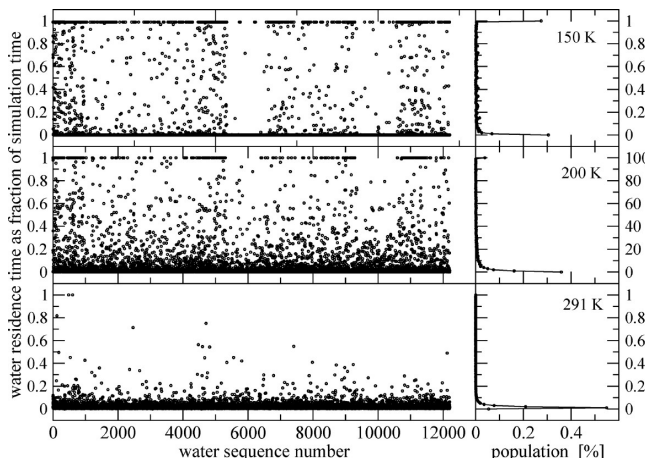


Figure 9. Residence times of 12 203 water molecules in the Crh crystal from the 19 ns trajectories at 150, 200, and 291 K (top to bottom). The residence time distributions are shown in the right-hand panels. A water molecule is considered to reside at the protein surface if the distance of its oxygen atom to any protein atom is smaller than 0.4 nm.

the β_3 strand (residues 40–43), and are exposed to solvent (Figure 1), which explains their higher mobility. The significantly larger RMSF of the C-terminal residues at 291 K is due to their exposure to the solvent. The C-terminus appears to be more flexible than the N-terminus which is immobilized by the β -sheet interactions of residues 2–8 (β_1) with residues 59–66 (β_4) of the other monomer of the dimer (see Figure 1).

Previous studies have shown, both theoretically^{39,57} and experimentally,^{58–60} that at about 200 K the properties of proteins display marked changes called a “glass transition”, which is, however, not the subject of the present study. Yet, the analysis of the mobility of solvent molecules may explain the temperature dependence of the motion of the protein atoms, as suggested in previous simulation studies^{40,41} where the solvent was found to induce motion of the protein atoms. We have carried out an analysis of the properties of the water in the Crh crystal, specifically its diffusion and rotational relaxation, to obtain insight in the mutual influence of the motions of protein and water.

Mobility of Water. Atom-Positional Fluctuations of Water Molecules in the Crh Crystal and in Bulk Water. In Figure 6, the positional RMSF of the 12203 water oxygen atoms in the crystal unit cell at 150, 200, and 291 K are shown. Note that the first 976 water molecules had as initial positions the water sites as identified in the crystal structure 1MU4. The mean square positional fluctuation (MSF) of a water molecule is proportional to its mean-square displacement (MSD)⁶¹

$$\text{MSF}(t) = \text{MSD}(t)/2 \quad (5)$$

and thus to its diffusion.

At a temperature of 150 K, the water molecules are largely immobilized ($\text{RMSF} < 0.04 \text{ nm}$) at their initial positions, and only a few water molecules have an RMSF larger than 0.2 nm. When the temperature is raised to 200 K, the water molecules do move more, but most of the water molecules still do not move more than 0.2 nm. The water molecules initially at the crystallographic water sites largely stay around these initial positions. The water molecules that show a low RMSF either remain immobilized in the bulk solvent or stay at the surface of the protein anchored by hydrogen bonds to the protein.

At 291 K, the mobility of the water molecules is significantly enhanced, while some water molecules still show low mobility because of their interaction with the protein surface. However, there is no difference in RMSF anymore between water molecules initially at crystallographic water sites or in the bulk. At 291 K, there are two regimes of mobility, of which a minority with smaller RMSF and a majority with larger RMSF, the former representing water molecules that are at the protein surface, the latter water molecules in the solvent regions of the crystal.

Since the mobility of water molecules as function of temperature will depend on the type of water model used, we have also studied the motion of SPC water molecules in bulk water; see Figure 7. At 300 K, the RMSF of water molecules show a Gaussian distribution centered at about 2 nm both at constant volume and at constant pressure. Decreasing the temperature changes the shape of the distribution and shifts it to lower RMSF values. At 250 K, in both simulations, the positional RMSF of the water molecules is composed of two distributions: one has the features of a Gaussian distribution

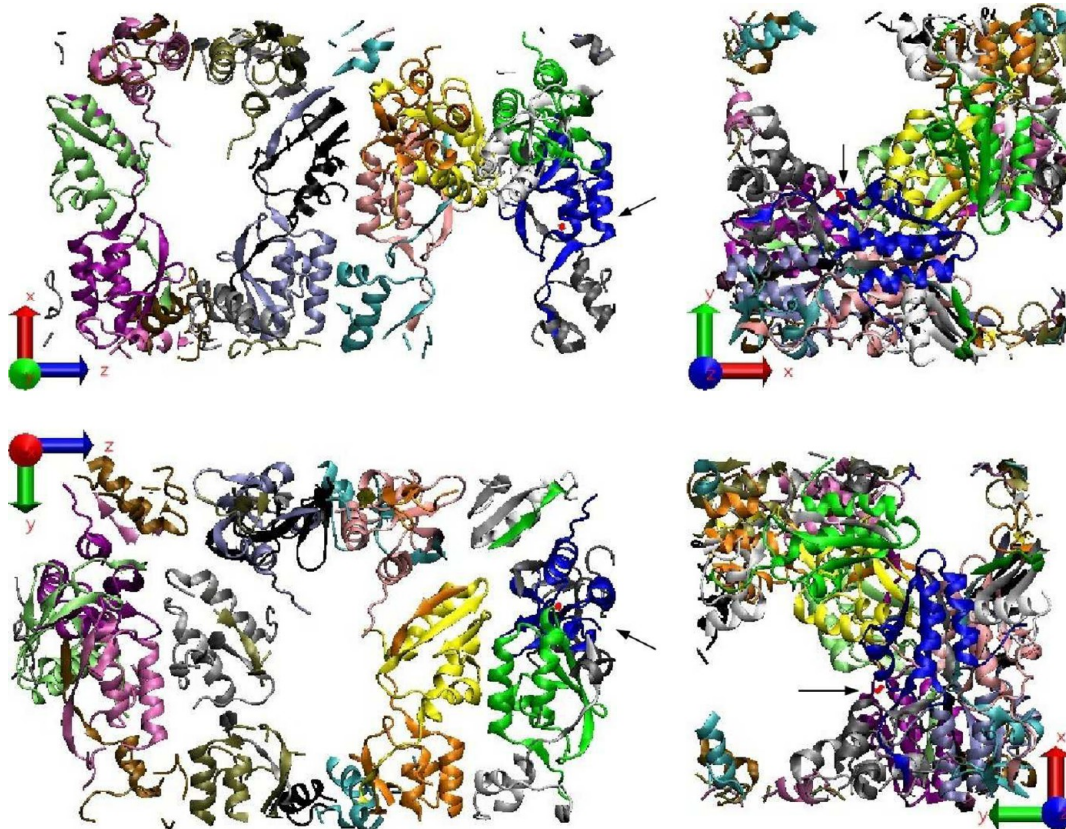


Figure 10. Low water mobility at 200 K: Projection on the zx -, xy -, zy -, and yx -planes of the 19-th ns trajectory of water 2 at 200 K. The trajectory of the water oxygen is represented as a red line (see the arrows), while the eight protein dimers in the crystal unit cell are shown in different colors. The diffusion coefficient of water 2 at 200 K is $4.3 \times 10^{-6} \text{ nm}^2 \text{ ps}^{-1}$.

centered at about 2 nm and another, relatively sharp distribution is centered at about 1 nm. When the temperature of the system is further decreased to 200 K, the mobility of the water molecules becomes restricted to 0.1–0.3 nm, that is, the diameter of a water molecule, and finally the water molecules are immobilized in place with an RMSF smaller than 0.05 nm and 0.01 at 150 and 100 K, respectively.

Water described by the SPC model does not solidify at 273 K but at the much lower $T_m = 190.5$ K shows a density maximum⁶² at 228 K instead of 277 K, and a larger diffusion coefficient of⁶³ $4.2 \times 10^{-3} \text{ nm}^2 \text{ ps}^{-1}$ than the experimental value⁶⁴ of $2.3 \times 10^{-3} \text{ nm}^2 \text{ ps}^{-1}$ at room temperature. Although the SPC model roughly reproduces the temperature dependence of water, it makes water too mobile thereby shifting its melting and glass transition temperatures downward compared to experiment. Yet, the temperature dependence of the SPC model in the range of 100–300 K shows that this model may be used to qualitatively describe the behavior of water at these temperatures. Comparing the distributions of the mobility of water molecules at the same temperature in the Crh crystal (Figure 6) and in bulk water (Figure 7), the same shape is observed at 150 K. Surprisingly, the water in the Crh crystal is more mobile than in bulk water at 200 K, while at 291 K the opposite is observed. The simulations at 200 K thus agree with the experimental findings that bulk water (“supernatant water” in ref 20) freezes much earlier than the water in vicinity of the proteins (“crystal water” in ref 20).

Diffusion of Water Molecules in the Crh Crystal and in Bulk Water. The diffusion coefficients of water are reported in Table 2, where the data are obtained as averages over all water

molecules in the systems, and in Figure 8, where the distributions of the diffusion coefficients of individual water molecules calculated using eq 1 are given.

With the decrease of the temperature, the diffusion of water in both Crh crystal and bulk water is slowed down monotonously. However, the temperature dependence is different in both environments. At 150 K, the water is frozen in both bulk water and the Crh crystal with very low values of the diffusion coefficient of $0.4 \times 10^{-5} \text{ nm}^2 \text{ ps}^{-1}$ in bulk water and a twice lower value of $0.2 \times 10^{-5} \text{ nm}^2 \text{ ps}^{-1}$ in crystal. At 291 K, the value in the Crh crystal is with $114 \times 10^{-5} \text{ nm}^2 \text{ ps}^{-1}$ three times lower than the value of $379 \times 10^{-5} \text{ nm}^2 \text{ ps}^{-1}$ in bulk water. In contrast, at 200 K the value of $8.7 \times 10^{-5} \text{ nm}^2 \text{ ps}^{-1}$ is about three times larger than the value of about $3 \times 10^{-5} \text{ nm}^2 \text{ ps}^{-1}$ in bulk water, confirming the observations made for the water atom-positional RMSF values.

Considering the distributions of the diffusion coefficients of the individual water molecules in the Crh crystal and in bulk water in Figure 8, the diffusion coefficient of water shows at 150 K in the Crh crystal a narrower distribution than in bulk water. A similar picture is observed at 291 K. However, at 200 K, the diffusion coefficients of water molecules in the Crh crystal show a broader distribution, with a longer tail, than in bulk water. This causes the averaged value of the diffusion coefficient of water in Crh to be larger than in bulk water at 200 K (Table 2).

At 291 K, there are still some water molecules in the Crh crystal that do not diffuse (see the inset of the panel at 291 K in Figure 8), while in bulk water no such molecules are found. These water molecules are bound by the interaction with the protein. Figure 9 shows the residence times of the 12 203 water

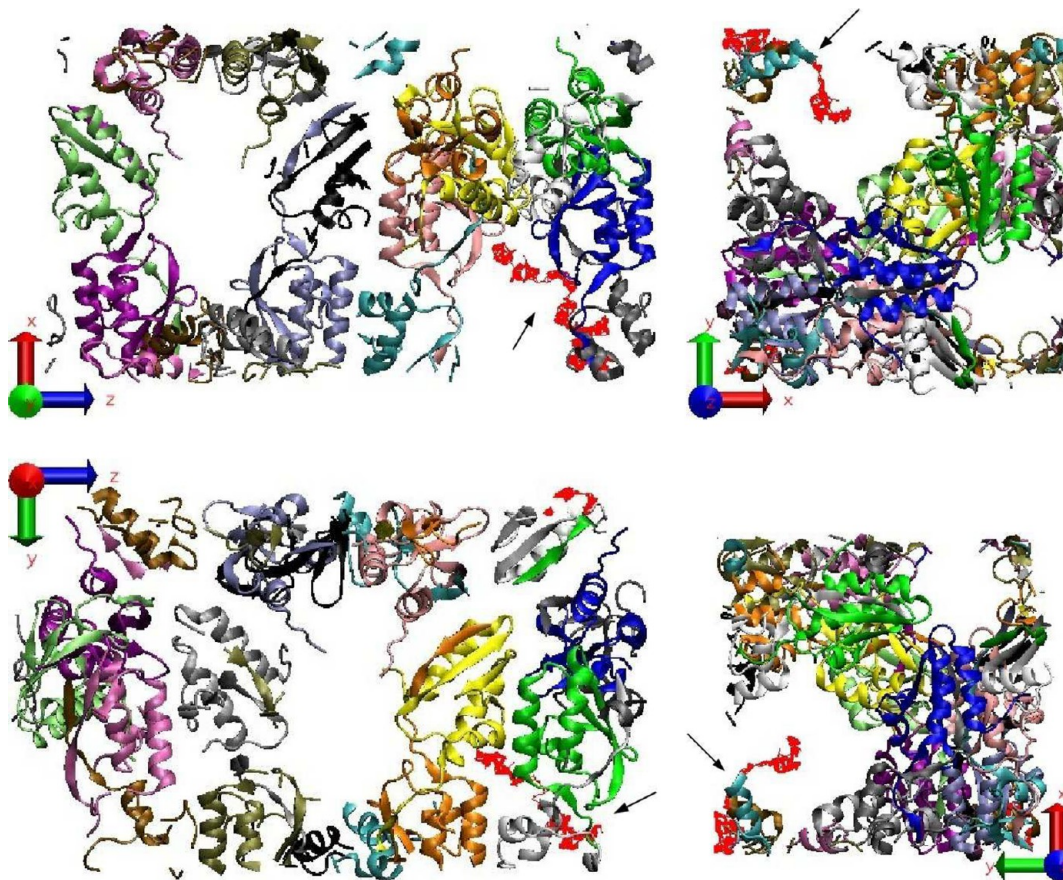


Figure 11. High water mobility at 200 K: Projection on the zx -, xy -, zy -, and yx - planes of the 19-th ns trajectory of water 2135 at 200 K. The trajectory of the water oxygen is represented as a red line (see the arrows), while the eight protein dimers in the crystal unit cell are shown in different colors. The diffusion coefficient of water 2135 at 200 K is $1.9 \times 10^{-3} \text{ nm}^2 \text{ ps}^{-1}$.

molecules at the protein surface, that is, their oxygen atom staying within a distance of 0.4 nm from a protein atom, as fraction of the total simulation time of 19 ns, and the residence time distribution at 150, 200, and 291 K. At 291 K, most residence times are well below 2 ps with only two water molecules completely immobile in the simulation, while at 200 K about 4% of the water molecules are completely immobile and at 150 K about 27%.

Influence of the Protein Environment on Water Mobility. It is known that nanoconfinement may change the properties of aqueous water and lower its melting temperature compared to the bulk and thus maintain a nanoenvironment for supercooled liquid water which may lead to abnormal behavior of water compared to bulk water. In such a nanoenvironment, water is surrounded by concave or convex surfaces composed of partially charged particles of which some, alkyl atoms, represent a hydrophobic environment while others, protein heteroatoms and ions, a hydrophilic one. In simulations of such systems, the topology of the surfaces may display fluctuations due to the motion of protein backbone or side-chain atoms and ions, especially at high temperatures. To investigate the influence of these factors on the diffusion of water, we have performed four additional simulations of the Crh crystal with all protein atoms (*pr*) or only their backbone atoms (*br*) positionally restrained and in addition the protein partial charges (*p0*) and ion charges (*i0*) set to zero. According to the data in Table 3, at 200 K, these changes in the environment of the water molecules do not have a significant impact on the diffusion of water. At 291 K

though, they tend to increase the diffusion of water, the major effect being due to the restraining of the motion of the protein backbone atoms.

Our analysis of the water mobility indicates that water molecules in crystalline Crh show different types of behavior on the time scale of the simulation. The trajectories of a few water molecules of high mobility, water 2656 at 291 K and water 2135 at 200 K, and of low mobility, water 166 at 291 K and water 2 at 200 K, are shown in Figures 10–13. We only show the water molecule that is to be presented and its protein environment, that is, the 16 monomers, and not the other 202 water molecules. The secondary structures of the protein dimers are drawn in different colors to distinguish them from each other. At 200 K and 291 K, the motion of the two water molecules with a low diffusion coefficient (Figures 10 and 12) is restricted to the surface of the proteins, while the two water molecules with a large diffusion coefficient (Figures 11 and 13) diffuse through the voids containing large patches of water between the proteins.

Rotational Relaxation Time of Water Molecules in the Crh Crystal and in Bulk Water. Table 2 presents the average rotational relaxation times τ_1 and τ_2 of the vectors $O-H_1$, $O-H_2$, H_1-H_2 , and the dipole moment μ of the water molecules in the Crh crystal and in bulk water, and their distributions are shown in Figures 14 and 15.

In bulk water at 291 K, the τ_1 and τ_2 values of the four molecular vectors were 3 and 1 ps, at constant volume as well as at constant pressure. When the temperature is lowered to 200

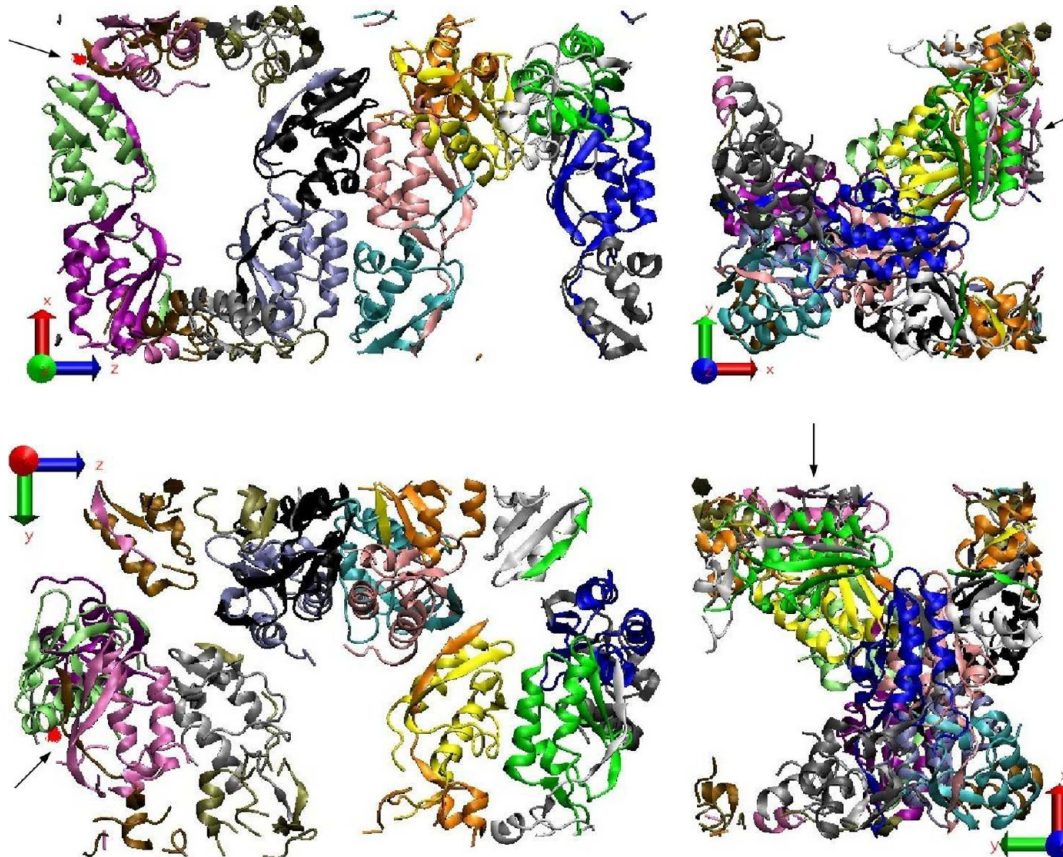


Figure 12. Low water mobility at 291 K: Projection on the zx-, xy-, zy-, and yx- planes of the 19-th ns trajectory of water 166 in the Crh crystal unit cell at 291 K. The trajectory of the water oxygen is represented as a red line (see the arrows), while the eight protein dimers in the crystal unit cell are shown in different colors. The diffusion coefficient of water 166 at 291 K is $7.6 \times 10^{-6} \text{ nm}^2 \text{ ps}^{-1}$.

K, the τ_1 and τ_2 from the constant volume simulation are almost two times as long as those from the constant pressure simulation. The longer average relaxation time in the constant volume simulation at 200 K is due to the broader distribution of τ_1 and τ_2 values at constant volume than at constant pressure. In contrast, at 291 K, both ensembles yield the same distribution for τ_1 and τ_2 . When the system is simulated at 150 K, the water molecules are immobilized, and within the time period of analysis no tumbling of the water molecules is observed.

Water behaves differently when comparing bulk water to water in the Crh crystal. In the latter environment water molecule tumbling is faster at 200 K and slightly slower at 291 K. At 291 K, the average τ_1 values for the vectors OH_1 , OH_2 , H_1H_2 , and μ of the water molecules in the Crh crystal are calculated to be 4.0, 4.0, 3.8, and 4.5 ps respectively. The tumbling of the dipole moment vector $\vec{\mu}$ is slightly slower compared to that of the other molecular vectors, as was also observed in a nanoconfined water-graphene system⁶⁵ and hydrocarbon–water systems,^{66,67} suggesting an electrostatic contribution to immobilization of water in the Crh crystal. At 200 K, the rotational relaxation time distributions in the Crh crystal are less wide than in bulk water (upper panels in Figures 14 and 15), whereas at 291 K the opposite is observed (lower panels).

Nanoconfinement has been observed to influence the properties of water. Recently, Choudhury⁶⁷ investigated the influence of the nanoconfinement and the surface topology of an alkane solute plate on the orientational dynamics of water

with water modeled by the SPC/E model⁶⁸ and the alkanes by the OPLS-UA force field,⁶⁹ and found that at 298 K the rotation of the water molecules in the confined region is not in agreement with the Debye isotropic rotational diffusion model⁷⁰ which may be due to the anisotropy of translational diffusion⁷¹ and thus of the rotational motion as well in the confined region. These results are consistent with our observations for the Crh crystal, and moreover, we observed an enhancement of this effect at 200 K.

As seen in Table 3, at 291 K, the use of positional restraints for the protein atoms does not have a significant influence on the τ_1 and τ_2 values of the water molecules while switching-off the protein atomic charge results in a small but noticeable acceleration of the rotational relaxation of water. The latter effect becomes more significant at 200 K. While protein restraining lengthens the orientational relaxation of the water molecules, switching-off the water–protein electrostatic interactions shortens the τ_1 and τ_2 values by more than a factor of 2. These results are consistent with those by Pizzitutti et al.⁴² for 9 ns MD simulations of the protein hen egg white lysozyme in water at 300 K using a CHARMM force field and SPC/E water. Rigidifying the protein had only a minor influence on water rotational relaxation, while switching off the electrostatic protein–water interactions shortens water rotational relaxation considerably.

At both temperatures, the few ions in the Crh crystal do not show much influence on the rotational relaxation time of water.

Experimental data on water rotational relaxation at the surface of small partially hydrophobic solutes in aqueous

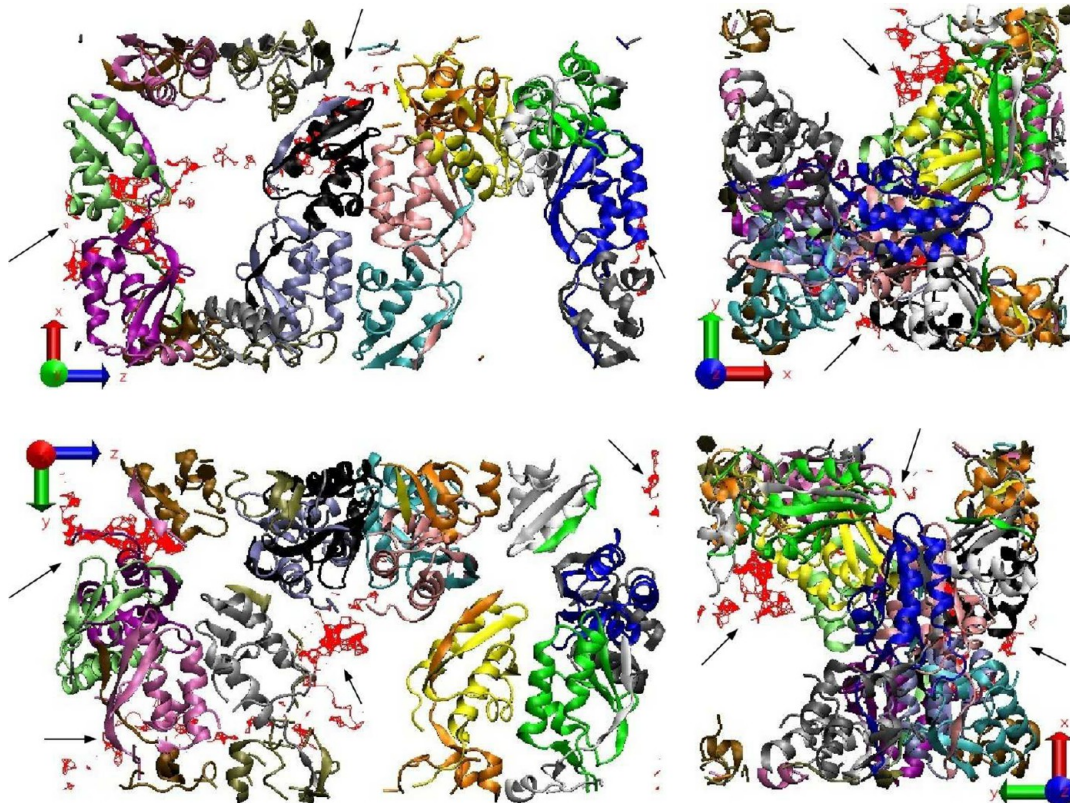


Figure 13. High water mobility at 291 K: Projection on the zx -, xy -, zy -, and yx -planes of the 19-th ns trajectory of water 2656 in the Crh crystal unit cell. The trajectory of the water oxygen is represented as a red line (see the arrows), while the eight protein dimers in the crystal unit cell are shown in different colors. The diffusion coefficient of water 2656 at 291 K is $1.6 \times 10^{-2} \text{ nm}^2 \text{ ps}^{-1}$.

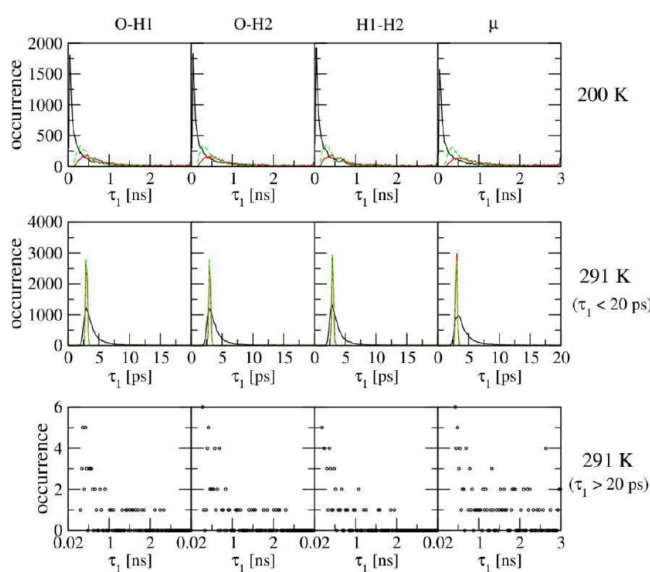


Figure 14. The distribution of the rotational relaxation time τ_1 of water vectors $O-H_1$, $O-H_2$, H_1-H_2 , and μ in the Crh crystal (in black) and in bulk water (in red constant volume and in green constant pressure) in the simulations at 200 and 291 K. At 291 K, in the Crh crystal the distribution of τ_1 has a long tail beyond 20 ps which represents less than 0.01% of total population. These τ_1 values are shown in the bottom panels.

solution has been obtained from ^2H NMR relaxation measurements.²¹ It was found that at room temperature water relaxation in the hydration shell of the solute is slowed down by a factor 1.5–2 relative to bulk water, whereas below

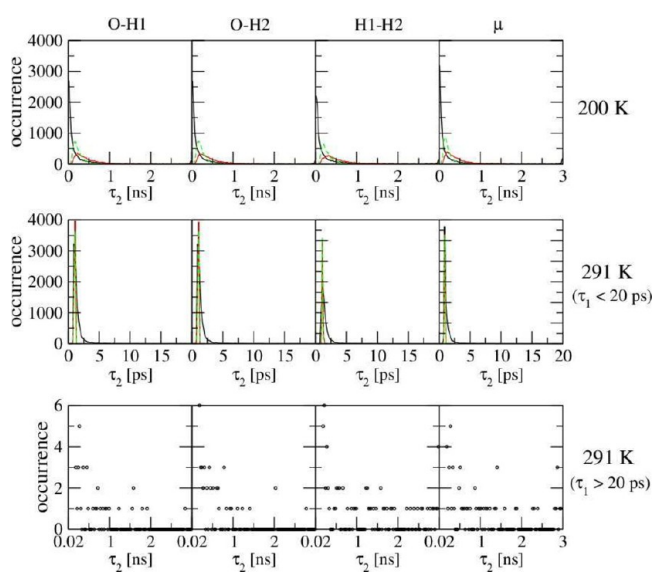


Figure 15. The distribution of the rotational relaxation time τ_2 of water vectors $O-H_1$, $O-H_2$, H_1-H_2 , and μ in the Crh crystal (in black) and in bulk water (in red constant volume and in green constant pressure) in the simulations at 200 and 291 K. At 291 K, in the Crh crystal the distribution of τ_2 has a long tail beyond 20 ps which represents less than 0.01% of total population. These τ_2 values are shown in the bottom panels.

237 K these water molecules rotate faster than bulk water. These results for noncrystalline small solutes are in agreement with our observations for the Crh crystal.

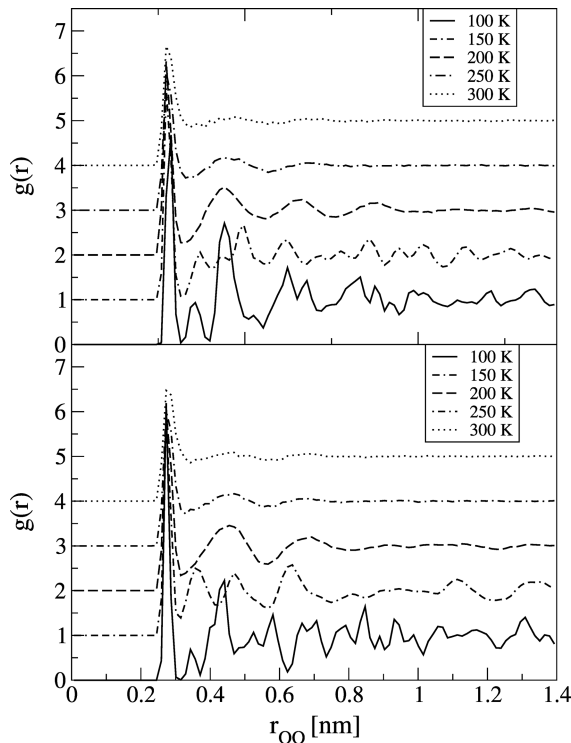


Figure 16. Oxygen–oxygen radial distribution function $g(r)$ of bulk water (5384 molecules) at different temperatures (100 K: solid; 150 K: dot-dash-dot; 200 K: dashed; 250 K: dot-dash; 300 K: dotted lines) in simulations at constant volume (upper panel) or constant pressure (lower panel). The curves at different temperatures are vertically shifted by one unit for a better visibility.

Low Temperature Properties of the SPC Water Model. Since the presented results for the behavior of water molecules in the crystal of the protein Crh at low temperature will depend on the characteristics of the SPC model for liquid water at low temperature, we calculated some properties of supercooled bulk water using the SPC model. Low temperature studies have been reported for the SPC/E model^{72–74} and the TIPSP model⁷⁵ but not for the SPC model.

The oxygen–oxygen radial distribution function (RDF) of water, an indicator of how the water molecules in the liquid are structured, is shown for bulk water simulations at 100, 150, 200, 250, and 300 K at constant volume and constant pressure in Figure 16.

At the higher temperatures of 250 and 291 K, the particular configurational ensemble, constant volume or pressure, does not show much influence on the radial structure of the liquid. When the temperature is lowered to 200 K, a fourth solvation shell becomes visible at constant volume while not yet in the isobaric simulation. When the temperature is lowered beyond 200 K, in both simulations the water molecules become more ordered.

Various thermodynamic properties of the SPC model at temperatures between 100 and 300 K are depicted in Figure 17.

Density ρ . At constant pressure, a density maximum (ρ_{\max}) is observed between 200 and 300 K; however, the resolution of 50 K of the temperature window used in the simulations is not sufficient to locate the temperature at which ρ_{\max} appears. In previous work,⁶² the density maximum of the liquid water was located at 228 K for the SPC model, which is about 37 K above

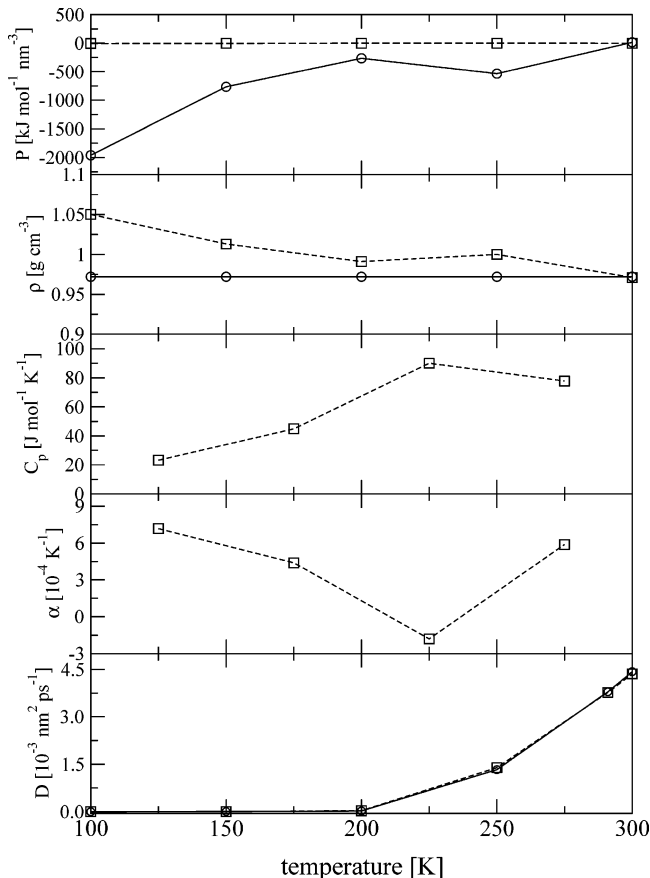


Figure 17. From top to bottom: pressure (P), density (ρ), heat capacity (C_p), thermal expansion coefficient (α) and diffusion coefficient (D) of bulk water (5384 molecules) as a function of temperature (T) in constant volume (solid) and constant pressure (dashed) simulations using the SPC water model.

the melting temperature⁷⁶ of 190 K of the SPC model. This is consistent with our results.

We note that a density minimum of bulk water at low temperature was only observed in computer simulations^{77–79} but not experimentally due to ice nucleation when the temperature decreases below 240 K. Such a density minimum also appears in our simulations between 150 and 250 K. Some studies^{77–80} indicate that a phase transition may exist in supercooled water, but this issue is beyond the scope of the present study, so we did not analyze a possible phase transition in the simulations of bulk water at low temperatures. At even lower temperatures, bulk water is in its solid phase, and further cooling leads to an increase of the density.

Thermal Expansion Coefficient α . From the definition of the thermal expansion coefficient which reads

$$\alpha = \frac{(\partial V / \partial T)_p}{V} = - \left(\frac{\ln(\rho_2 / \rho_1)}{T_2 - T_1} \right)_p \quad (6)$$

where ρ_1 and ρ_2 are the densities at temperatures T_1 and T_2 , the thermal expansivity of liquid water is zero at 277 K, below or above which it becomes negative or positive. This is qualitatively reproduced in our constant pressure simulations from which the α is calculated to be -0.00018 K^{-1} at 225 and 0.00059 K^{-1} at 275 K. A minimum of α has been proposed⁸¹ at 225 K. This would support the hypothesis that large-scale fluctuations in water correlation functions dominate the

dynamics of water anomalies.⁸² However, the concept of inhomogeneous water on the 1-nm-length scale has been challenged⁸³ by the argument that current available spectroscopic data (Raman, IR, XAS, XES, etc.) are not sufficient to imply a two-state behavior of water and to overrule the traditional roughly tetrahedral picture of liquid water.

Our analysis of the properties of bulk water shows that the SPC model provides a qualitatively sound description of the behavior of water at low temperature.

CONCLUSION

By means of MD simulations, the mobility of water in crystalline Crh was studied and compared with that of bulk or neat water at three temperatures, 150, 200, and 291 K. This investigation was invoked by the NMR experimental observation of water mobility in the crystal of Crh at temperatures far below 273 K.

At 150 and 291 K, both translational and rotational motion of the water molecules in the Crh crystal is slowed down compared to bulk water, while at 200 K, a temperature close to the “glass transition” of water and solvated proteins, the motion of water molecules in the protein crystal is enhanced compared to bulk water. This is in line with the observation from NMR experiments on hydrophobic solutes in water that water reorientation at the solute surface is faster than in bulk at temperatures below 237 K. The properties of the proteins were artificially changed, that is, by rigidifying the protein backbones or all protein atoms and by removing electrostatic interactions between the proteins and water in order to detect a particular feature of the Crh crystal that could cause the relatively high water mobility in the Crh crystal at low temperature. Of these factors, rigidifying the protein backbones slightly enhanced water diffusion, while it slowed down rotation. In contrast, removal of electrostatic protein–water interactions did not change water diffusion but enhanced rotational motion significantly. The current results confirm the anomalous water mobility in the Crh crystal at 200 K but do not yield a single cause of it.

ASSOCIATED CONTENT

Supporting Information

The atom-positional root-mean-square deviations from the X-ray structure (Figure S1) and root-mean-square fluctuations (Figure S2) of the protein side-chain non-hydrogen atoms. This material is available free of charge via the Internet at <http://pubs.acs.org>.

AUTHOR INFORMATION

Corresponding Authors

*(D.W.) E-mail: dwang@ihep.ac.cn.

*(W.F.v.G.) E-mail: wfvgn@igc.phys.chem.ethz.ch.

Present Address

¹Institute of High Energy Physics, Chinese Academy of Sciences, 100049 Beijing, China.

Notes

The authors declare no competing financial interest.

ACKNOWLEDGMENTS

The authors thank Bertil Halle for a critical reading of the manuscript, the Swiss National Science Foundation, Grant Numbers 200020-131827 and 200020-124611, its National Competence Center for Research (NCCR) in Structural

Biology, the Agence Nationale de la Recherche (ANR SIMI8 2012), and the European Research Council, Grant Number 228076, for financial support. D.W. thanks the Chinese Academy of Sciences for funding in the framework of a Frontier of Novelty program, Grant Numbers Y1515540U1 and Y2291810S3.

REFERENCES

- (1) Franks, F., Ed. *Water: A Comprehensive Treatise*; Plenum Press: New York, 1972.
- (2) Franks, F. *Polywater*; MIT Press: Cambridge, USA, 1981.
- (3) Alder, B. J.; Wainwright, T. E. Phase transition for a hard sphere system. *J. Chem. Phys.* **1957**, *27*, 1208–1209.
- (4) Alder, B. J.; Wainwright, T. E. Studies in molecular dynamics. I. General method. *J. Chem. Phys.* **1959**, *31*, 459–466.
- (5) Rahman, A.; Stillinger, F. H. Molecular dynamics study of liquid water. *J. Chem. Phys.* **1971**, *55*, 3336–3359.
- (6) Guillot, B. A reappraisal of what we have learnt during three decades of computer simulations on water. *J. Mol. Liq.* **2002**, *101*, 219–260.
- (7) Berendsen, H. J. C.; Postma, J. P. M.; van Gunsteren, W. F.; Hermans, J. In *Intermolecular Forces*; Pullman, B., Ed.; Reidel: Dordrecht, 1981; pp 331–342.
- (8) Mahoney, M. W.; Jorgensen, W. L. A five-site model for liquid water and the reproduction of the density anomaly by rigid, nonpolarizable potential functions. *J. Chem. Phys.* **2000**, *112*, 8910–8922.
- (9) Rick, S. W. Simulations of ice and liquid water over a range of temperatures using the fluctuating charge model. *J. Chem. Phys.* **2001**, *114*, 2276–2283.
- (10) Kunz, A. P.; van Gunsteren, W. F. Development of a non-linear classical polarisation model for liquid water and aqueous solutions: COS/D. *J. Phys. Chem. A* **2009**, *113*, 11570–11579.
- (11) Bukowski, R.; Szalewicz, K.; Groenenboom, G. C.; van der Avoird, A. Predictions of the properties of water from first principles. *Science* **2007**, *315*, 1249–1252.
- (12) Lo Conte, L.; Chothia, C.; Janin, J. The atomic structure of protein-protein recognition sites. *J. Mol. Biol.* **1999**, *285*, 2177–2198.
- (13) Rodier, F.; Bahadur, R. P.; Chakrabarti, P.; Janin, J. Hydration of protein-protein interfaces. *Proteins* **2005**, *60*, 36–45.
- (14) de Vlieg, J.; Berendsen, H. J. C.; van Gunsteren, W. F. An NMR based molecular dynamics simulation of the interaction of the lac repressor headpiece and its operator in aqueous solution. *Proteins* **1989**, *6*, 104–127.
- (15) Reddy, C. K.; Das, A.; Jayaram, B. Do water molecules mediate protein-DNA recognition. *J. Mol. Biol.* **2001**, *314*, 619–632.
- (16) Lu, Y.; Wang, R.; Yang, C. Y.; Wang, S. Analysis of ligand-bound water molecules in high-resolution crystal structures of protein-ligand complexes. *J. Chem. Inf. Model.* **2007**, *47*, 668–675.
- (17) Panigrahi, S.; Desiraju, G. R. Strong and weak hydrogen bonds in the protein-ligand interface. *Proteins* **2007**, *67*, 128–141.
- (18) Penin, F.; Favier, A.; Montserret, R.; Brutscher, B.; Deutscher, J.; Marion, D.; Galinier, A. Evidence for a dimerisation state of the bacillus subtilis catabolite repression hpr-like protein, crh. *J. Mol. Microbiol. Biotechnol.* **2001**, *3*, 429–432.
- (19) Juy, M.; Penin, F.; Favier, A.; Galinier, A.; Montserret, R.; Haser, R.; Deutscher, J.; Böckmann, A. Dimerization of Crh by reversible 3D domain swapping induces structural adjustments to its monomeric homologue Hpr. *J. Mol. Biol.* **2003**, *332*, 767–776.
- (20) Böckmann, A.; Gardiennet, C.; Verel, R.; Hunkeler, A.; Loquet, A.; Pintacuda, G.; Emsley, L.; Meier, B.; Lesage, A. Characterization of different water pools in solid-state NMR protein samples. *J. Biomol. NMR* **2009**, *45*, 319–327.
- (21) Qvist, J.; Halle, B. Thermal signature of hydrophobic hydration dynamics. *J. Am. Chem. Soc.* **2008**, *130*, 10345–10353.
- (22) Koga, K.; Gao, G. T.; Tanaka, H.; Zeng, X. C. Formation of ordered ice nanotubes inside carbon nanotubes. *Nature* **2001**, *412*, 802–805.

- (23) Bai, J.; Wang, J.; Zeng, X. C. Multiwalled ice helices and ice nanotubes. *Proc. Natl. Acad. Sci. U.S.A.* **2006**, *103*, 19664–19667.
- (24) Giovambattista, N.; Rossky, P. J.; Debenedetti, P. G. Phase transitions induced by nanoconfinement in liquid water. *Phys. Rev. Lett.* **2009**, *102*, 050603.
- (25) Badyal, Y. S.; Saboungi, M. L.; Price, D. L.; Shastri, S. D.; Haefner, D. R.; Soper, A. K. Electron distribution in water. *J. Chem. Phys.* **2000**, *112*, 9206–9208.
- (26) Dellago, C.; Naor, M. M. Dipole moment of water molecules in narrow pores. *Comput. Phys. Commun.* **2005**, *169*, 36–39.
- (27) Senapati, S.; Chandra, A. Dielectric constant of water confined in a nanocavity. *J. Phys. Chem. B* **2001**, *105*, 5106–5109.
- (28) Dokter, A. M.; Woutersen, S.; Bakker, H. J. Inhomogeneous dynamics in confined water nanodroplets. *Proc. Natl. Acad. Sci. U.S.A.* **2006**, *103*, 15355–15358.
- (29) Lucent, D.; Vishal, V.; Pande, V. S. Protein folding under confinement: A role for solvent. *Proc. Natl. Acad. Sci. U.S.A.* **2007**, *104*, 10430–10434.
- (30) Mancinelli, R.; Bruni, F.; Ricci, M. A. Controversial evidence on the point of minimum density in deeply supercooled confined water. *J. Phys. Chem. Lett.* **2010**, *1*, 1277–1282.
- (31) Garofalini, S. H.; Mahadevan, T. S.; Xu, S.; Scherer, G. W. Molecular mechanisms causing anomalously high thermal expansion of nanoconfined water. *ChemPhysChem* **2008**, *9*, 1997–2001.
- (32) Crupi, V.; Interdonato, S.; Longo, F.; Majolino, D.; Migliardo, P.; Venuti, V. A new insight on the hydrogen bonding structures of nanoconfined water: a raman study. *J. Raman Spectrosc.* **2008**, *39*, 244–249.
- (33) Ockwig, N. W.; Cygan, R. T.; Criscenti, L. J.; Nenoff, T. M. Molecular dynamics studies of nanoconfined water in clinoptilolite and heulandite zeolites. *Phys. Chem. Chem. Phys.* **2008**, *10*, 800–807.
- (34) Mancinelli, R. The effect of confinement on water structure. *J. Phys.: Condens. Matter* **2010**, *22*, 404213.
- (35) Zhang, H.; Ye, H.; Zheng, Y.; Zhang, Z. Prediction of the viscosity of water confined in carbon nanotubes. *Microfluid. Nanofluid.* **2011**, *10*, 403–414.
- (36) Ye, H.; Zhang, H.; Zhang, Z.; Zheng, Y. Size and temperature effects on the viscosity of water inside carbon nanotubes. *Nanoscale Res. Lett.* **2011**, *6*, 87.
- (37) Pomata, M. H. H.; Sonoda, M. T.; Skaf, M. S.; Elola, M. D. Anomalous dynamics of hydration water in carbohydrate solutions. *J. Phys. Chem. B* **2009**, *113*, 12999–13006.
- (38) Stirnemann, G.; Sterpone, F.; Laage, D. Dynamics of water in concentrated solutions of amphiphiles: key roles of local structure and aggregation. *J. Phys. Chem. B* **2011**, *115*, 3254–3262.
- (39) Vitkup, D.; Ringe, D.; Petsko, G. A.; Karplus, M. Solvent mobility and the protein ‘glass’ transition. *Nat. Struct. Mol. Biol.* **2000**, *7*, 34–38.
- (40) Karplus, M.; McCammon, J. A. Molecular dynamics simulations of biomolecules. *Nat. Struct. Biol.* **2002**, *9*, 646–652.
- (41) Karplus, M.; McCammon, J. A. Corrigendum: molecular dynamics simulations of biomolecules. *Nat. Struct. Biol.* **2002**, *9*, 788–788.
- (42) Pizzitutti, F.; Marchi, M.; Sterpone, F.; Rossky, P. J. How protein surfaces induce anomalous dynamics of hydration water. *J. Phys. Chem. B* **2007**, *111*, 7584–7590.
- (43) Matthews, B. W. Solvent content of protein crystals. *J. Mol. Biol.* **1968**, *33*, 491–497.
- (44) Schuler, L. D.; Daura, X.; van Gunsteren, W. F. An improved GROMOS96 force field for aliphatic hydrocarbons in the condensed phase. *J. Comput. Chem.* **2001**, *22*, 1205–1218.
- (45) van Gunsteren, W. F.; Billeter, S. R.; Eising, A. A.; Hünenberger, P. H.; Krüger, P.; Mark, A. E.; Scott, W. R. P.; Tironi, I. G. *Biomolecular Simulation: The GROMOS96 Manual Und User Guide*; Vdf Hochschulverlag AG, ETH Zürich: Zürich, Switzerland, 1996.
- (46) Scott, W. R. P.; Hünenberger, P. H.; Tironi, I. G.; Mark, A. E.; van Gunsteren, W. F. The gromos biomolecular simulation program package. *J. Phys. Chem. A* **1999**, *103*, 3596–3607.
- (47) Christen, M.; Hünenberger, P. H.; Bakowies, D.; Baron, R.; Bürgi, R.; Geerke, D. P.; Heinz, T. N.; Kastenholz, M. A.; Kräutler, V.; Oostenbrink, C.; Peter, C.; Trzesniak, D.; van Gunsteren, W. F. The GROMOS software for biomolecular simulation: GROMOS05. *J. Comput. Chem.* **2005**, *26*, 1719–1751.
- (48) <http://www.gromos.net>.
- (49) Hockney, R. W. The potential calculation and some applications. *Methods Comput. Phys.* **1970**, *9*, 136–211.
- (50) Ryckaert, J. P.; Cicotti, G.; Berendsen, H. J. C. Numerical integration of the cartesian equations of motion of a system with constraints: Molecular dynamics of *n*-alkanes. *J. Comput. Phys.* **1977**, *23*, 327–341.
- (51) Barker, J. A.; Watts, R. O. Monte Carlo studies of the dielectric properties of water-like models. *Mol. Phys.* **1973**, *26*, 789–792.
- (52) Tironi, I. G.; Sperb, R.; Smith, P. E.; van Gunsteren, W. F. A generalized reaction field method for molecular dynamics simulations. *J. Chem. Phys.* **1995**, *102*, 5451–5459.
- (53) Heinz, T. N.; van Gunsteren, W. F.; Hünenberger, P. H. Comparison of four methods to compute the dielectric permittivity of liquids from molecular dynamics simulations. *J. Chem. Phys.* **2001**, *115*, 1125–1136.
- (54) Berendsen, H. J. C.; Postma, J. P. M.; van Gunsteren, W. F. Molecular dynamics with coupling to an external bath. *J. Chem. Phys.* **1984**, *81*, 3684–3690.
- (55) Kabsch, W.; Sander, C. Dictionary of protein secondary structure: Pattern recognition of hydrogen-bonded and geometrical features. *Biopolymers* **1983**, *22*, 2577–2637.
- (56) Walser, R.; Mark, A. E.; van Gunsteren, W. F. On the temperature and pressure dependence of a range of properties of a type of water model commonly used in high-temperature protein unfolding simulations. *Biophys. J.* **2000**, *78*, 2752–2760.
- (57) Kurkal-Siebert, V.; Agarwal, R.; Smith, J. C. Hydration-dependent dynamical transition in protein: Protein interactions at ~240 k. *Phys. Rev. Lett.* **2008**, *100*, 138102.
- (58) Doster, W.; Cusack, S.; Petry, W. Dynamical transition of myoglobin revealed by inelastic neutron scattering. *Nature* **1989**, *337*, 754–756.
- (59) Srager, V.; Reinisch, L.; Champion, P. M. Investigation of laser-induced long-lived states of photolyzed MbCO. *Biochemistry* **1991**, *30*, 4886–4895.
- (60) Nocek, J. M.; Zhou, J. S.; De Forest, S. D.; Priyadarshy, S.; Beratan, D. N.; Onuchic, J. N.; Hoffman, B. M. Theory and practice of electron transfer within protein-protein complexes: application to the multidomain binding of cytochrome c by cytochrome c peroxidase. *Chem. Rev.* **1996**, *96*, 2459–2489.
- (61) Heiner, A. P. *Predictive aspects of molecular dynamics simulations for proteins: Application to subtilisin BPN*; Ph.D. Thesis; University of Groningen: The Netherlands, 1992.
- (62) Vega, C.; Abascal, J. L. F. Relation between the melting temperature and the temperature of maximum density for the most common models of water. *J. Chem. Phys.* **2005**, *123*, 144504.
- (63) Glättli, A.; Daura, X.; van Gunsteren, W. F. Derivation of an improved simple point charge model for liquid water: SPC/A and SPC/L. *J. Chem. Phys.* **2002**, *116*, 9811–9828.
- (64) Krynicki, K.; Green, C. D.; Sawyer, D. W. Pressure and temperature dependence of self-diffusion in water. *Faraday Discuss. Chem. Soc.* **1978**, *66*, 199–208.
- (65) Martí, J.; Nagy, G.; Guardia, E.; Gordillo, M. C. Molecular dynamics simulation of liquid water confined inside graphite channels: Dielectric and dynamical properties. *J. Phys. Chem. B* **2006**, *110*, 23987–23994.
- (66) Chowdhary, J.; Ladanyi, B. M. Water/hydrocarbon interfaces: Effect of hydrocarbon branching on single-molecule relaxation. *J. Phys. Chem. B* **2008**, *112*, 6259–6273.
- (67) Choudhury, N. Orientational dynamics of water trapped between two nanoscopic hydrophobic solutes: A molecular dynamics simulation study. *J. Chem. Phys.* **2010**, *133*, 154515.
- (68) Berendsen, H.; Grigera, J.; Straatsma, T. The missing term in effective pair potentials. *J. Phys. Chem.* **1987**, *91*, 6269–6271.

- (69) Jorgensen, W. L.; Madura, J. D.; Swenson, C. J. Optimized intermolecular potential functions for liquid hydrocarbons. *J. Am. Chem. Soc.* **1984**, *106*, 6638–6646.
- (70) Berne, B. J.; Pecora, R. *Dynamic Light Scattering: With Applications to Chemistry, Biology and Physics*; Wiley: New York, 1976.
- (71) Choudhury, N. Dynamics of water at the nanoscale hydrophobic confinement. *J. Chem. Phys.* **2010**, *132*, 064505.
- (72) Giovambattista, N.; Angell, C. A.; Sciortino, F.; Stanley, H. E. Glass-transition temperature of water: A simulation study. *Phys. Rev. Lett.* **2004**, *93*, 047801.
- (73) Giovambattista, N.; Debenedetti, P. G.; Sciortino, F.; Stanley, H. E. Structural order in glassy water. *Phys. Rev. E* **2005**, *71*, 061505.
- (74) Giovambattista, N.; Angell, C. A.; Sciortino, F.; Stanley, H. E. Structural relaxation in the glass transition region of water. *Phys. Rev. E* **2005**, *72*, 011203.
- (75) Mazza, M. G.; Giovambattista, N.; Starr, F. W.; Stanley, H. E. Relation between rotational and translational dynamic heterogeneities in water. *Phys. Rev. Lett.* **2006**, *96*, 057803.
- (76) Vega, C.; Sanz, E.; Abascal, J. L. F. The melting temperature of the most common models of water. *J. Chem. Phys.* **2005**, *122*, 114507.
- (77) Brovchenko, I.; Geiger, A.; Oleinikova, A. Multiple liquid-liquid transitions in supercooled water. *J. Chem. Phys.* **2003**, *118*, 9473–9476.
- (78) Brovchenko, I.; Geiger, A.; Oleinikova, A. Liquid-liquid phase transitions in supercooled water studied by computer simulations of various water models. *J. Chem. Phys.* **2005**, *123*, 044515–044531.
- (79) Paschek, D. How the liquid-liquid transition affects hydrophobic hydration in deeply supercooled water. *Phys. Rev. Lett.* **2005**, *94*, 217802–217806.
- (80) Poole, P.; Becker, S.; Sciortino, F.; Starr, F. Dynamical behavior near a liquid-liquid phase transition in simulations of supercooled water. *J. Phys. Chem. B* **2011**, *115*, 14176–14183.
- (81) Mallamace, F. The liquid water polymorphism. *Proc. Natl. Acad. Sci. U.S.A.* **2009**, *106*, 15097–15098.
- (82) Huang, C.; Wikfeldt, K.; Tokushima, T.; Nordlund, D.; Harada, Y.; Bergmann, U.; Niebuhr, M.; Weiss, T. M.; Horikawa, Y.; Leetmaa, M.; Ljungberg, M.; Takahashi, O.; Lenz, A.; Ojamae, L.; Lyubartsev, A. P.; Shin, S.; Pettersson, L. G. M.; Nilsson, A. The inhomogeneous structure of water at ambient conditions. *Proc. Natl. Acad. Sci. U.S.A.* **2009**, *106*, 15214–15218.
- (83) Soper, A. K.; Teixeira, J.; Head-Gordon, T. Is ambient water inhomogeneous on the nanometer-length scale? *Proc. Natl. Acad. Sci. U.S.A.* **2010**, *107*, E44.